

# Polarization spectroscopic analysis of noise produced in a turbulent plasma upon annihilation of oppositely moving magnetic fields

M.V. Babykin, A.I. Zhuzhunashvili, E.A. Oks, V.V. Shapkin, and G.V. Sholin

*I. V. Kurchatov Institute of Atomic Energy*

(Submitted August 28, 1972; resubmitted March 14, 1973)

Zh. Eksp. Teor. Fiz. 65, 175-188 (July 1973)

An optical technique for measuring the directivity pattern of electrostatic noise is described, based on a polarization analysis of the Stark contours of hydrogen spectral lines. The turbulence level of noise arising on annihilation of oppositely moving magnetic fields is measured by this technique and it is shown that a current instability at the electron-cyclotron-frequency harmonics arises in the plasma.

1. Spectroscopic plasma diagnostics based on the Stark effect has recently been increasingly employed in plasma turbulence studies. Progress in this direction has been a result of the development of electron-optical spectrochronography,<sup>[1,2]</sup> which can be used to examine spectral line profiles emitted by tenuous plasma during a single discharge, and also a result of the application of the theory of Stark broadening in the electric fields of turbulent oscillations,<sup>[3]</sup> which is a generalization of the theory of broadening in laminar plasma.

In early work, the analysis of experimental data was based on theoretical models which assumed that the distribution of noise in plasma was spherically symmetric. This was used to determine the nature and amount of turbulence associated with electrostatic noise in  $\theta$  pinches,<sup>[4]</sup> direct discharges,<sup>[5]</sup> and beam-plasma systems.<sup>[6]</sup> However, it was not long before Zavoiskii et al.<sup>[7]</sup> showed that the spectral line profile was a function of the polarization within the profile, and that this effect could be used to determine the angular distribution of noise. This distribution is very sensitive to the nature of the plasma instabilities and is therefore a decisive factor in the selection of theoretical models claiming to be capable of explaining experimental data. The present paper is devoted to the further development of polarization analysis of Stark hydrogen line profiles as a means of determining the electric fields in turbulent plasma oscillations.

Polarization analysis of Stark spectral line profiles is based on the difference between the longitudinal and transverse Stark effects, i.e., the preferential grouping of the  $\sigma$  components near the line center, and the more distant location of the  $\pi$  components in the wing. When the level of turbulence is sufficiently high, the adiabatic effect of the electric fields associated with plasma oscillations on the radiating atom gives rise to strong modulation of the light wave and, therefore, the influence of these oscillations on the line profile should be susceptible to treatment by the quasistatic theory over a major part of the line profile.<sup>[8]</sup> One must therefore first consider the influence of anisotropic electrostatic noise on the Stark hydrogen line profiles within the framework of the quasistatic approximation.<sup>[9]</sup>

2. Suppose that turbulent noise is expected in a system in which the  $z$  axis is the axis of symmetry. Its angular distribution should, of course, be axially symmetric, but the level of turbulence and the nature of the noise anisotropy are unknown. The spectral line profiles  $S_1(x)$  and  $S_2(x)$  are measured for two positions of the polaroids (1—parallel to the axis of the system and 2—at right-angles to it). In order to establish the anisotropy effect we consider the difference  $D(x) = S_1 - S_2$  for the

two profiles, where  $x = \lambda - \lambda_0$  is the departure from the line center in Å.

The electric field distribution will be described by the axially symmetric function  $W(E, \cos \vartheta)$ , where

$$\int_{E=0}^{\infty} \int_{\cos \vartheta=-1}^{+1} W(E, \cos \vartheta) dE d \cos \vartheta = 1.$$

In the quasistatic approximation, the line profile is proportional to the field distribution:

$$S_i(x) = \sum_{k, \nu} \int_{E=0}^{\infty} \int_{\cos \vartheta=-1}^{+1} \int_{u=-\infty}^{+\infty} W(E, \cos \vartheta) I_{k, \nu} f_{i \nu}(\cos \vartheta) \times \delta(x - E \Delta_{k, \nu} - u d) M(u) du d \cos \vartheta dE. \quad (1)$$

In these expressions the subscript  $i$  corresponds to position 1 or 2 of the polaroid, and the subscript  $\nu$  corresponds to the  $\pi$  or  $\sigma$  components, respectively. The second term in the argument of the  $\delta$  function is the Stark shift, where

$$\Delta_{k, \nu} = \frac{3ea_0\lambda_0^2}{4\pi c\hbar} [n(n_1 - n_2) - n'(n_1' - n_2')]$$

is the Stark constant,  $a_0$  is the Bohr radius,  $n$  is the principal quantum number, and  $n_1$  and  $n_2$  are the electric quantum numbers. The third term is the shift due to the Doppler effect, where  $d = v_0 \lambda_0 / c$  is the Doppler width and  $v_0 = (2T/M)^{1/2}$  is the mean thermal velocity of the atoms in the direction of the line of sight. The averaging with respect to the velocity is carried out over the Maxwellian distribution

$$M(u) du = \pi^{-1/2} e^{-u^2} du \quad (u = v_x / v_0).$$

The set of four functions  $f_{i \nu}(\cos \vartheta)$  describes the angular dependence of the observed Stark-component intensity. These functions can readily be determined by considering the projections along the polaroid directions 1 and 2 of the radiating dipole which either lies along the field  $\mathbf{E}$  ( $\pi$  component) or rotates in the plane perpendicular to  $\mathbf{E}$  ( $\sigma$  component)

$$f_{1\pi} = 3 \cos^2 \vartheta, \quad f_{2\pi} = 3/2(1 - \cos^2 \vartheta), \quad f_{1\sigma} = 3/2(1 - \cos^2 \vartheta), \quad f_{2\sigma} = 3/4(1 + \cos^2 \vartheta). \quad (2)$$

The functions  $f_{i \nu}$  are normalized so that the areas under the profiles  $S_1(x)$  and  $S_2(x)$  are equal to unity. In this we use the following general property of relative intensities  $I_{k \nu}$  of the Stark components:

$$\sum_k I_{k\pi} = 1/2, \quad \sum_k I_{k\sigma} = 1/2. \quad (3)$$

The difference profile  $D(x)$  contains only the linear combinations

$$f_{1\pi} - f_{2\pi} = 3/2(3 \cos^2 \vartheta - 1), \quad f_{1\sigma} - f_{2\sigma} = 3/4(1 - 3 \cos^2 \vartheta).$$

If we substitute

$$I_{k\pi} = 3I_{k\pi}, \quad I_{k\sigma} = -^3/2I_{k\sigma}, \quad (4)$$

we can omit the subscript  $\nu$  in the course of summation in Eq. (1), since now the angular factor is independent of  $\nu$ :

$$D(x) = \sum_k \int_{E=0}^{\infty} \int_{\cos\theta=-1}^{+1} \int_{u=-\infty}^{+\infty} W(E, \cos\theta) I_k^{1/2} (3 \cos^2\theta - 1) \times \delta(x - E\Delta_k - ud) M(u) du d\cos\theta dE =$$

$$= \sum_k I_k \int_{E=0}^{\infty} \int_{u=-\infty}^{+\infty} F(E) M(u) \delta(x - E\Delta_k - ud) du dE, \quad (5)$$

$$F(E) = \int_{-1}^{+1} W(E, \cos\theta)^{1/2} (3 \cos^2\theta - 1) d\cos\theta. \quad (6)$$

Consider the case when the Doppler broadening is small in comparison with the Stark shift for all the side components. To within terms of the second order in  $d/\Delta_k \langle E \rangle$  we then have

$$D(x) = \sum_k \frac{I_k}{|\Delta_k|} F\left(\frac{x}{\Delta_k}\right) + \frac{I_0}{d} M\left(\frac{x}{d}\right) \int_0^{\infty} F(E) dE. \quad (7)$$

Apart from a narrow central part, this profile represents the usual Stark broadening of a spectral line by quasistatic fields. Only the intensities of the Stark components change sign in accordance with Eq. (4), and the role of the "isotropic" distribution function is assumed by  $F(E)$ . This function has a simple physical interpretation. It shows whether fields of given amplitude  $E$  have a preferred direction and the extent to which this direction is more probable than all the others. For the isotropic noise distribution,  $F(E) = 0$ . Any departure from isotropy results in  $F(E)$  being different from zero, and this difference increases with increasing anisotropy of the noise distribution. If the angular field distribution is elongated along the axis of the system then  $F(E) > 0$ , and if it is compressed in that direction then  $F(E) < 0$ .

Let

$$S_F = \int_0^{\infty} F(E) dE.$$

The "norm"  $S_F$  of the function  $F(E)$  depends only on the degree of anisotropy  $\eta = \langle E_z^2 \rangle / \langle E_x^2 \rangle$  and is independent of the scale of the fields. The function  $S_F(\eta)$  increases monotonically from  $S_F(0) = -1/2$  to  $S_F(\infty) = +1$ , and  $S_F(1) = 0$ .

To obtain specific results we must introduce certain specific assumptions with regard to the distribution  $W(E, \cos\theta)$  of the quasistatic electric fields in the plasma. Let us take as a model the superposition of a one-dimensional noise spectrum with wave vectors lying along the axis of the system, and a two-dimensional spectrum with wave vectors lying in the plane perpendicular to this axis. Each of these spectra is the superposition of a large number of oscillations with random phases. The amplitude distribution in each of them will therefore be given by the corresponding Rayleigh functions:

$$W_1(E_{\parallel}) dE_{\parallel} = [2\pi \langle E_{\parallel}^2 \rangle]^{-1/2} \times \exp\left(-\frac{1}{2} \frac{E_{\parallel}^2}{\langle E_{\parallel}^2 \rangle}\right) dE_{\parallel}, \quad (8)$$

$$W_2(E_{\perp}) dE_{\perp} = \frac{E_{\perp}}{\langle E_{\perp}^2 \rangle} \times \exp\left(-\frac{E_{\perp}^2}{\langle E_{\perp}^2 \rangle}\right) dE_{\perp}. \quad (9)$$

As a rule, the case which is interesting from the experimental point of view is that where the mean fields  $\langle \vec{E} \rangle$  of the electrostatic oscillations are much greater than the mean fields  $E_0$  due to the individual ions. The contribution of the individual particles to the quasistatic

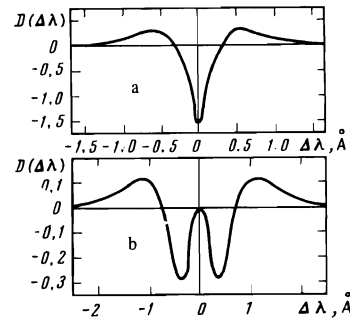


FIG. 1. Difference profiles for the Balmer lines  $H_{\alpha}$  (a) and  $H_{\beta}$  (b) with  $E_z/E_x = 3$ ,  $E_x = 20$  kV/cm,  $d = 0.1 \text{ \AA}$ .

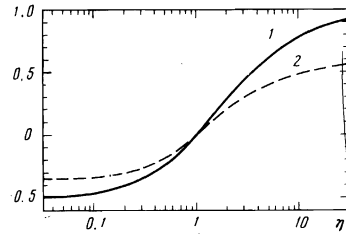


FIG. 2. Dependence of the universal function  $S_F$  and of the function  $S_D$  for the  $H_{\alpha}$  line on the degree of anisotropy  $\eta$ : 1— $S_F$ ; 2— $S_D$ .

field distribution can then be regarded as negligible, and the distribution of the resultant field  $E = E_{\parallel} + E_{\perp}$  can be written in the form

$$W(E, \cos\theta) dE d\cos\theta = \int W_1(E_{\parallel}) W_2(E_{\perp}) \delta(E - E_{\parallel} - E_{\perp}) dE_{\parallel} dE_{\perp} d\cos\theta = \left[ \frac{2}{\pi \langle E_{\parallel}^2 \rangle} \right]^{1/2} \frac{E^2}{\langle E_{\perp}^2 \rangle} \times \exp\left\{-E^2 \left[ \frac{1}{\langle E_{\perp}^2 \rangle} + \left( \frac{1}{2\langle E_{\parallel}^2 \rangle} - \frac{1}{\langle E_{\perp}^2 \rangle} \right) \cos^2\theta \right]\right\} dE d\cos\theta. \quad (10)$$

The geometric representation of this distribution is an ellipsoid of revolution with the axis along the  $z$  axis. As the degree of anisotropy  $\eta = [2\langle E_{\parallel}^2 \rangle / \langle E_{\perp}^2 \rangle]^{1/2}$  increases from 0 to  $\infty$ , the shape of this ellipsoid changes from a highly oblate "lens" to a highly prolate "sausage." It is spherical when  $\eta = 1$ .<sup>1)</sup>

Within the framework of this model the function  $F(E)$  and, consequently, the difference profile  $D(x)$  can be written analytically in the form

$$F(E) = \frac{E^2}{\sqrt{8\pi} E_x E_x^2} \exp\left(-\frac{E^2}{2E_x^2}\right) \left\{ \Phi\left[\frac{3}{2}, \frac{5}{2}, \frac{1}{2}(E_x^2 - E_x^{-2})E^2\right] - \Phi\left[\frac{1}{2}, \frac{3}{2}, \frac{1}{2}(E_x^2 - E_x^{-2})E^2\right] \right\}, \quad (11)$$

where  $\Phi(\alpha, \gamma, t)$  represents the degenerate hypergeometric functions. Finally, we have the simple analytic formula

$$S_F(\eta) = \frac{\eta^2 + 1/2}{\eta^2 - 1} - \frac{3}{2} \frac{\eta^2}{(\eta^2 - 1)^{3/2}} \begin{cases} \arcsin(1 - \eta^{-2})^{1/2}, & \eta > 1 \\ \ln(\eta^{-1} + (\eta^2 - 1)^{1/2})^{-1}, & \eta < 1 \end{cases} \quad (12)$$

Figure 1 shows a typical form of the calculated difference profile for the  $H_{\alpha}$  and  $H_{\beta}$  lines. This figure was obtained for the "sausage" type field distribution. For anisotropy of the opposite sign ("lens" distribution) the picture must be rotated about the abscissa axis. It follows that from a single difference profile we can immediately determine, at least qualitatively, the spatial distribution of noise.

The areas  $S_D$  corresponding to the upper and lower parts of the profile  $D(x)$  are equal to one another and proportional to  $S_F(\eta)$ , i.e., they depend only on the de-

gree of anisotropy. Because of the different positions of the  $\pi$  components in the wing relative to the  $\sigma$  components grouped near the center, the functions  $S_D(\eta)$  are different for different lines. The clearest differentiation between the  $\pi$  and  $\sigma$  components occurs for the first series terms ( $L_\alpha, H_\alpha, P_\alpha, \dots$ ). Hence their difference profiles are the most sensitive functions of anisotropy. Figure 2 shows the functions  $S_F(\eta)$  and  $S_D(\eta)$  for the  $H_\alpha$  line. If we know the normalized polarization profiles  $S_1(x)$  and  $S_2(x)$  for the  $H_\alpha$  line, we can determine the area  $S_D$  corresponding to the lower or upper halves of the difference profile  $D(x)$ , and then use the graph given in Fig. 2 to determine the degree of anisotropy  $\eta = E_Z/E_X$ .

The difference profile enables us to find not only the ratio  $E_Z/E_X$  but also each of these fields separately. The quantity  $E_{\max} = \max(E_Z/E_X)$  can be estimated from the position of the distant extremum  $X_{\text{extr}}$  of the difference profile

$$E_{\max} \sim \frac{X_{\text{extr}}}{\Delta_n}, \quad \Delta_n^2 = \sum_k I_{kn}/\Delta_k^p / \sum_k I_{kn}/\Delta_k^{p+1}, \quad p = \begin{cases} 1, & \eta > 1 \\ 2, & \eta < 1. \end{cases}$$

The quantity  $E_{\max}$  can be determined more precisely from the intensity distribution in the wing:

$$D_{AS}(x) \infty \begin{cases} \exp(-x^2/2E_{\max}^2 \Delta_n^2), & D_{AS}(x) > 0 \\ -x \exp(-x^2/2E_{\max}^2 \Delta_n^2), & D_{AS}(x) < 0 \end{cases}$$

The polarization method of determining the noise anisotropy can also be used even when the Doppler broadening exceeds the Stark broadening. In this case, we can expand the  $\delta$  function in Eq. (5) in terms of the parameter  $\Delta_k \langle E \rangle / d$ . The result is

$$D(x) = \sum_k \frac{I_k}{d} \int_0^\infty dE F(E) \left\{ 1 + \frac{\Delta_k}{d} E \frac{d}{du} + \frac{1}{2} \left( \frac{\Delta_k}{d} \right)^2 E^2 \frac{d^2}{du^2} + \dots \right\} M(u) \Big|_{u=x/d}. \quad (13)$$

This expression contains sums of the form

$$\sum_k I_k (\Delta_k)^q, \quad q = 0, 1, 2.$$

Since  $\tilde{I}_{-k} = +\tilde{I}_k$  and  $\Delta_{-k} = -\Delta_k$ , these sums differ from zero only for even  $q$ . Moreover, according to Eqs. (3) and (4),  $\sum \tilde{I}_k = 0$  and to within terms of the fourth order in  $\Delta_k \langle E \rangle / d$ , we have

$$D(x) = \left( 2 \frac{x^2}{d^2} - 1 \right) \frac{\exp(-x^2/d^2)}{\sqrt{\pi} d} \left[ \sum_k \frac{1}{2} \frac{\Delta_k^2}{d^2} \int_0^\infty F(E) E^2 dE \right]. \quad (14)$$

Thus, when  $d \gg \Delta_k \langle E \rangle$ , the difference profile is small ( $\propto \Delta_k^2 \langle E \rangle / d^2$ ) in comparison with the polarization profiles  $S_1(x)$ . Figure 3 shows a typical form of this difference profile for the  $H_\alpha$  and  $H_\beta$  lines. This figure was obtained for the sausage-type distribution. By rotating the figure about the abscissa axis we obtain the lens case. Consequently, even when isotropic Doppler broadening masks the polarization effects, one can still determine the nature of the noise distribution. Moreover, the vertical scale of the profile  $D(x)$  can be used to determine

$$\int_0^\infty F(E) E^2 dE = E_z^2 - E_x^2$$

and hence find  $E_{\max}$  provided the anisotropy is not too small. Since, however, Doppler broadening tends to reduce the amount of information in the polarization profile for which  $d > \Delta_k \langle E \rangle$ , it is more reasonable to examine experimentally the higher terms of the Balmer series, where  $\langle E \rangle \Delta_k > d$  (the Stark constant  $\alpha d \propto \lambda_0$  and decreases with increasing  $n$ ).

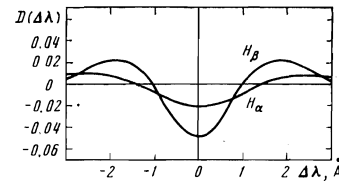


FIG. 3. Difference profiles for  $E_Z/E_X = 3$ ,  $E_X = 2$  kV/cm and radiating-atom temperature  $T_\alpha \approx 300$  eV.

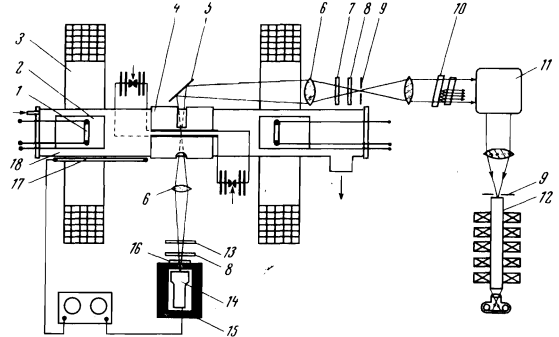


FIG. 4. The Dimpol installation: 1—cathode, 2—anode, 3—field coils, 4—pulsing circuit, 5—mirror, 6—focusing lenses, 7—polaroid, 8—light filter, 9—spectrograph slit, 10—Fabry-Perot interferometer, 11—ISP-51 spectrograph, 12—electron-optical converter, 13—diaphragm, 14—FEU-52 photomultiplier, 15—magnetic shield for the photomultiplier, 16—polarization filter, 17—magnetic probe, 18—vacuum chamber.

3. The measurements were carried out on the "Dimpol" installation.<sup>[10]</sup> A Penning discharge (Fig. 4) was used to generate the initial plasma in the magnetic mirror system with a mirror ratio of two. The application of an alternating magnetic field of large amplitude, produced by a rapid discharge, resulted in the appearance of the turbulent state in the current layer separating the opposing magnetic fields of predetermined strength.

The experiment was carried out in continuously flowing hydrogen (pressure  $4 \times 10^{-3} - 10^{-2}$  Torr). The plasma density was determined from the microwave cutoff at wavelengths of 4, 8, and 15 mm, and varied in the range  $10^{13} - 1.7 \times 10^{13}$  cm<sup>-3</sup> during the development of the turbulence. The amplitude of the alternating magnetic field was measured with a probe located near the pulsing circuit. Light was taken out both at right-angles to the axis (transverse observation) and along the axis (longitudinal observation), and was projected onto the slit of the spectrograph. We used crossed dispersion of the Fabry-Perot interferometer IT-51-30 and the ISP-51 spectrograph. The interference orders of the spectral lines were projected onto the photocathode of a scanned five-stage electron-optical converter UMI-95 (this is the method of electron-optical spectrochronography). The interferometer spacing ring was 0.3 mm thick, which produced a dispersion interval  $\Delta\lambda_S = 7.2$  Å and  $\Delta\lambda_S = 3.9$  Å for the  $H_\alpha$  and  $H_\beta$  lines, respectively. The image on the screen of the electron-optical converter was photographed on AÉRO-1300 film. Blackening to intensity conversion was based on a densitometer curve obtained with set of neutral filters.

Turbulent plasma was investigated under the following conditions: alternating magnetic field amplitude  $\tilde{H} = 2.8 - 4.2$  kOe, constant magnetic field  $H_0 = 0.7$  kOe. During the first half-period the field  $H_0$  and  $\tilde{H}$  were antiparallel. In the initial plasma the  $H_\alpha$  and  $H_\beta$  profiles

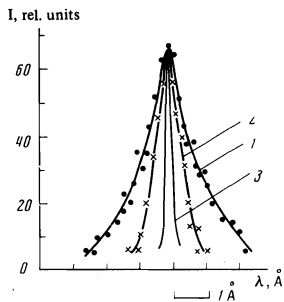


FIG. 5. Doppler profiles of the  $H_{\alpha}$ : 1—profile drawn after the pulsing circuit was switched off, 2—profile for the initial plasma, 3—instrumental profile.

were broadened mainly by the Doppler effect and their half-widths were 1 and 0.8 Å. The instrumental width for the  $H_{\alpha}$  line was determined from the broadening of the 6328 Å helium-neon laser line and was found to be  $\Delta\lambda_{1/2} = 0.3$  Å (see Fig. 5). For the  $H_{\beta}$  line the instrumental width was determined from the profile emitted by a hydrogen lamp, and was also not greater than 0.3 Å.

When the pulsing circuit was switched on, the spectral lines were found to broaden very substantially, with the  $H_{\beta}$  broadened more than the  $H_{\alpha}$ , as expected from the Stark broadening mechanism. Figure 6 shows spectrochronograms for two interference orders obtained in the case of  $H_{\alpha}$  and  $H_{\beta}$  at neutral hydrogen pressure  $p_0 \approx 4 \times 10^{-3}$  torr,  $n_e = 1.2 \times 10^{13}$  cm $^{-3}$ ,  $H_0 = 0.7$  kOe, and  $\tilde{H} = 4.2$  Oe for transverse observation. It is clear that, in the presence of turbulence, the broadening of the  $H_{\beta}$  was so considerable that the orders were smeared out, i.e., the line half-width exceeded  $\Delta\lambda_S = 3.9$  Å. As the amplitude of the alternating field  $\tilde{H}$  was reduced, the  $H_{\alpha}$  and  $H_{\beta}$  half-widths at the time of turbulence development were found to decrease. To avoid the overlap of the interference orders we used the smaller value  $\tilde{H} \approx 2.8$  kOe in subsequent experiments.

Figure 7 shows the  $H_{\alpha}$  profile at the instant of development of the turbulence (indicated by the points) together with the theoretical profile calculated for different noise distributions. Curve 2 shows the profile calculated for isotropic low-frequency turbulence. The quasistatic profile of the Stark side components was described in this case by the three-dimensional Rayleigh distribution

$$W_s(E) dE = 3 \left( \frac{6}{\pi} \right)^{1/2} \frac{E^2}{(\langle E^2 \rangle)^{3/2}} \exp \left( - \frac{3}{2} \frac{E^2}{\langle E^2 \rangle} \right) dE,$$

where  $\langle E^2 \rangle \equiv \tilde{E}^2$  is the mean square of the field in the low-frequency electrostatic oscillations. (The contribution of electric fields due to the individual particles need not be taken into account because  $\tilde{E} \gg E_0 = 2.6$  eN $^{2/3}$ .) The profile of the central Stark component was assumed in these calculations to be Gaussian with a half-width given by the Doppler broadening, since electron collision broadening was negligible for these particular plasma parameters.

The best agreement between the profile calculated in this way and the experimental profile is observed for the half-width  $\Delta\lambda_{1/2} \approx 2.9$  Å of the Gaussian central component, and for the root mean square field of the turbulent oscillations amounting to  $\sim 70$  kV/cm (curve 2 in Fig. 7). This value of  $\tilde{E}$  corresponds to a noise level higher than one would expect from simple theoretical estimates. Moreover, the Doppler half-width of the  $H_{\alpha}$  measured immediately after switching off the pulsing circuit, when charge-transfer processes have not as yet succeeded in reducing the temperature of the ions and the radiating atoms, whilst noise relaxation has not yet

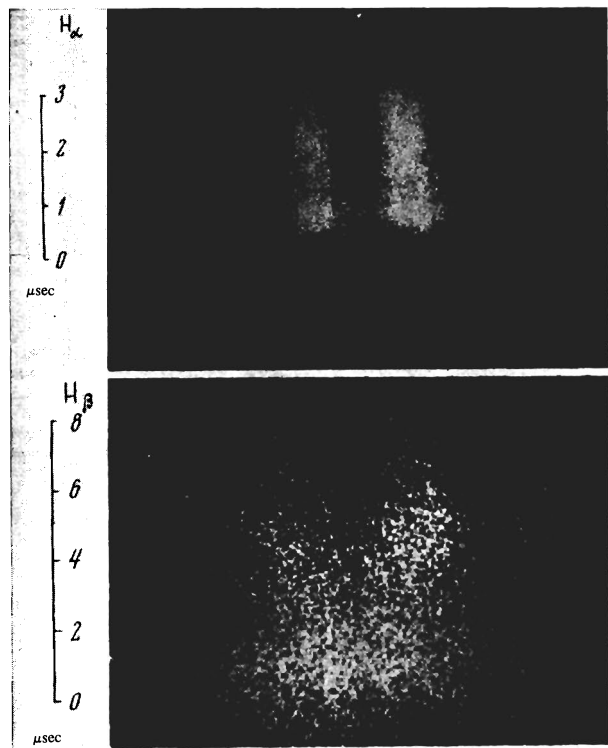


FIG. 6. Spectrochronogram of the  $H_{\alpha}$  and  $H_{\beta}$  interference orders: pressure  $p_0 = 4 \times 10^{-3}$  torr,  $n_e = 1.2 \times 10^{13}$  cm $^{-3}$ ,  $H_0 = 0.7$  kOe,  $\tilde{H} = 4.2$  kOe.

set in, amounts to  $\Delta\lambda_{1/2} \approx 2$  Å and not 2.9 Å. The latter figure follows from analysis of spectrochronograms performed on the assumption of an isotropic noise distribution. This casts doubt on the validity of the model in which the noise distribution is assumed to be isotropic, and forces us to consider more adequate models.

Under the conditions of our experiments the isotropization of noise may not have taken place because the current producing the instability did not have an axial component. It is natural to suppose that the noise may not, therefore, have had an axial component and was confined essentially to the plane perpendicular to the axis of the system. Calculations have shown (see below) that, with this type of noise anisotropy, the line profiles emitted in the transverse direction with the polarization vectors along the axis of the system ( $z$  polarization) and perpendicular to it ( $\varphi$  polarization) will be different in width. Moreover, the profile with the  $\varphi$  polarization will be different in width. Moreover, the profile with the  $\varphi$  polarization is broader than that with the  $z$  polarization and the profile with isotropic noise calculated for the same mean noise level. At the same time, a check on the polarizing properties of the optical system shows that the equipment transmits practically all the  $\varphi$ -polarized light ( $I_{\varphi}/I_z = 6.25$ ). This was largely connected with the polarizing effect of the reflecting mirror (see Fig. 4).

Since most of the radiation recorded during the experiment was  $\varphi$ -polarized, it was natural to carry out a comparison with the corresponding theoretical profile. The profile was calculated with the side component profile described by the two-dimensional radial distribution. The best agreement was observed for the Doppler half-width  $\Delta\lambda_{1/2} = 2.2$  Å and root mean square field of the turbulent oscillations  $\tilde{E} \approx 35$  kV/cm (curve 1 in Fig. 7). It follows that the assumption of anisotropic distribution

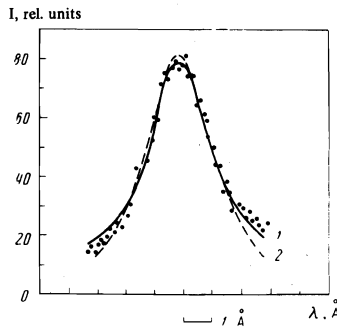


FIG. 7. Experimental  $H_\alpha$  profile (points) compared with calculations: 1—anisotropic turbulence, 2—isotropic turbulence. Plasma parameters as in Fig. 6.

of electric fields in unstable oscillations leads to a more reasonable noise level for the Doppler half-width, which is in good agreement with measurements immediately after the pulsing circuit is switched off. Of course, the agreement between this calculated profile and the experimental profile cannot be regarded as a definite indication that the noise distribution is anisotropic. Polarization analysis is still essential and has been carried out by introducing a polarizer into the optical system which can be used to isolate the  $z$  and  $\varphi$  polarizations in the case of transverse observation, and the  $\varphi$  and  $r$  polarizations in the case of longitudinal observation.

Measurements of the normalized  $r$ ,  $z$ , and  $\varphi$  polarization profiles are necessary before comparison with the theory can be carried out. The normalization was carried out using a natural source of light which was, in fact, the beam-plasma discharge. The normalization was achieved by introducing a neutral filter (NS-7) with attenuation by a factor of 6.25 when the  $\varphi$  polarization profile was recorded. Since the  $z$  and  $\varphi$  profiles were recorded in successive discharges, it was necessary to monitor the light and choose frames with equal  $H_\alpha$  intensities. The monitor was a photomultiplier with an interference filter mounted in front of the cathode. The photomultiplier signal was recorded on an oscillograph screen. This procedure yielded the  $S_z$  and  $S_\varphi$  profiles of the  $H_\alpha$ , and these were used to obtain the difference profile (Fig. 8).

The observed intensity could have been affected by unpolarized light emitted by internal regions in which plasma was not turbulent and, therefore, normalization of the  $S_i(\Delta\lambda)$  to unity gives a difference profile  $D(\Delta\lambda)$  whose norm  $S_D(\Delta\lambda)$  is, in general, less than that corresponding to the given degree of anisotropy. This uncertainty does not appear, however, if the normalization is based on the absolute intensity in the wings of the difference profile, which are exclusively due to the turbulent plasma:

$$D_{AS}(\Delta\lambda) = \begin{cases} \left(\frac{2}{\pi}\right)^{1/2} \frac{1}{E_{max}(1-\eta^2)} \sum_{k>0} \frac{\tilde{f}_{k\pi}}{\Delta_{k\pi}} \exp\left(-\frac{x^2}{2\Delta_{k\pi}^2 E_{max}^2}\right), & \eta > 1 \\ -\frac{x}{2E_{max}^2(1-\eta^2)^{1/2}} \sum_{k>0} \frac{\tilde{f}_{k\pi}}{\Delta_{k\pi}^2} \exp\left(-\frac{x^2}{2\Delta_{k\pi}^2 E_{max}^2}\right), & \eta < 1 \end{cases}, \quad (15)$$

$$E_{max}^2 \equiv \max(\langle E_z^2 \rangle, \langle E_\varphi^2 \rangle, \langle E_r^2 \rangle).$$

This expression contains the quantity  $\eta$ , which is unknown. By choosing quite arbitrarily some specific scale for the ordinate axis we can determine the modulus of  $S_D(\Delta\lambda)$  in these relative units and hence the ratio  $S_D(\eta)/D_{AS}(\Delta\lambda)$  taken at the arbitrary point  $(\Delta\lambda)_0$  in the wing which will not, of course, depend on the chosen

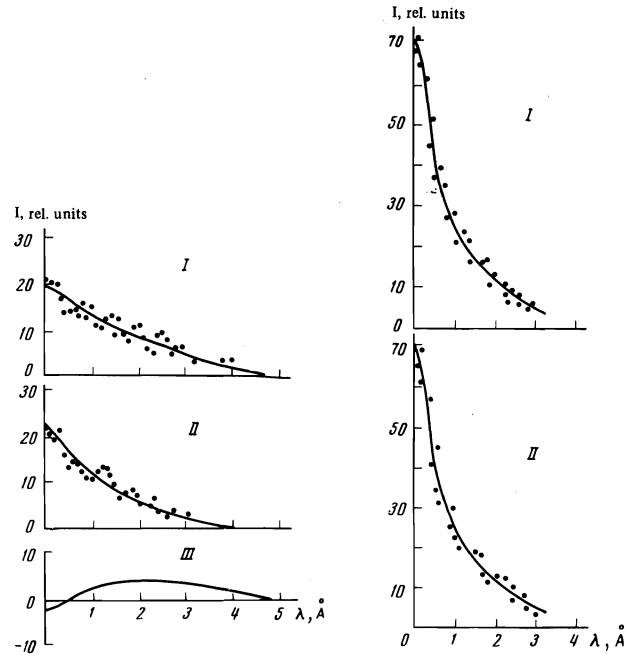


FIG. 8

FIG. 9

FIG. 8. Polarization  $H_\alpha$  profiles for transverse observation ( $p_0 = 4 \times 10^{-3}$  Torr,  $H_0 = 0.7$  kOe,  $H = 3$  kOe): I— $\varphi$  polarization, II— $z$  polarization, III—difference profile.

FIG. 9. Polarization  $H_\alpha$  profiles for longitudinal observation: I— $r$  polarization, II— $\varphi$  polarization.

units. Consequently, the experimental difference profile enables us to determine the quantity

$$S_D \text{ rel}(\eta) = S_D(\eta) \begin{cases} 1 - \eta^{-2}, & \eta > 1 \\ (1 - \eta^2)^{1/2}, & \eta < 1 \end{cases}$$

The experimental data (see Fig. 5, curve 3) can then be used to conclude that the corresponding polarization corrections are small, i.e., in the transverse direction the light is emitted largely by the turbulent plasma, and the low-frequency electrostatic noise develops preferentially in the plane perpendicular to the magnetic field:

$$E_{\parallel} = E_z = 8 \text{ kV/cm}, \quad E_{\perp} = (E_\varphi^2 + E_r^2)^{1/2} = 30 \text{ kV/cm}.$$

However, transverse observations cannot be used to conclude anything about the ratio of the turbulent electric fields in the  $r$  and  $\varphi$  directions. At the same time, there are theoretical models which predict different anisotropy along these directions: for the ion-acoustic instability the noise should be mainly elongated in the direction of the current ( $\varphi$ ), while noise in directions perpendicular to the current ( $r$  and  $z$ ) should be much smaller and should have roughly the same amplitude.<sup>[11]</sup> On the other hand, if current dissipation occurs as a result of development of instability at the lower hybrid frequency, or at the harmonics of the electron cyclotron frequency, the amplitude of the oscillation fields in the direction of the current ( $\varphi$ ) and in the direction of the electric field due to charge separation ( $r$ ) should be equal, and the amplitude of the oscillations along the magnetic field should be small.<sup>[12-14]</sup> Therefore, longitudinal observations should substantially increase the amount of information which can be deduced about the nature of the developing noise.

Figure 9 shows the  $r$  and  $\varphi$  polarization profiles in the case of longitudinal observation, obtained under the

same conditions as the profiles in Fig. 5 (pressure  $p_0 = 4 \times 10^{-3}$  Torr,  $n = 1.2 \times 10^{13}$  cm $^{-3}$ ,  $H_0 = 0.7$  kOe,  $H = 3$  kOe). The longitudinally observed profiles are narrower than those observed in the transverse direction. This difference is due to the substantial contribution to the total line intensity of regions with nonturbulent plasma in the case of longitudinal observation. Analysis of the intensity distribution in the wing in the case of longitudinal observations yields  $\tilde{E} \approx 25$  kV/cm, which is in agreement with the estimated  $E_\varphi$  obtained from transverse observations. As regards the difference profile, this is found to be practically zero, which suggests that the electric fields in the  $r$  and  $\varphi$  directions are equal.

The polarization analysis of Stark line profiles emitted by turbulent plasma can thus be used to determine the noise level and its angular distribution. The use of the polarization method is restricted by the condition that the electric microfields, which have the broadening effect, must be quasistatic. It is well known that, at sufficient distances from the line center, the broadening is always quasistatic in nature. The necessary condition for this is merely that the modulation depth of the radiated light wave due to the fluctuating microfields is sufficiently high, i.e.,  $d \cdot E / \hbar \omega \gg 1$ . For frequencies in the region of the plasma ion frequency  $\omega_{pi} = (4\pi Ne^2/M)^{1/2}$  and the electron cyclotron frequency  $\omega_{He} = eH/mc$ , the quasistatic condition is satisfied for distances from the line center

$$\Delta\lambda = \lambda_0 \frac{\Delta\omega}{\omega_0} = \Delta\lambda \frac{dE}{\hbar\omega_0} \gg \frac{\omega_{He}}{\omega_0} \lambda_0 \approx 0.05 \text{ \AA}.$$

It is clear from Fig. 5 that most of the difference profile lies in this region.

For the profile as a whole, the quasistatic condition can be regarded as satisfied only when the lifetime of the atom in the given Stark state is less than the period of variation in the turbulent electric field, i.e.,

$$\gamma \approx 3\pi N_e \frac{\hbar^2 n^4}{m^2 v_{Te}} \ln \frac{\rho_{max}}{\rho_{min}} \gg \omega.$$

It is readily verified that, under our experimental conditions, and for frequencies  $\omega \leq 10^9$  sec $^{-1}$ , there may be observable deviations from the quasistatic condition which will be appreciable in the central part of the line with  $\Delta\lambda \leq 0.05$  \AA. One would therefore expect that the experimental and calculated profiles would differ in the central part. Most of the information about the spectrum and the degree of turbulence is contained, however, in the part of the difference profile which lies above the abscissa and governs the intensity in the wing. In fact, according to the above theory, the degree of asymmetry can be deduced either from the area of the difference profile lying above the abscissa axis or the area of the profile lying below it, because these two areas are equal. At the same time, the upper part of the profile is completely described by the quasistatic theory, whereas for the lower part the theory may turn out to be inadequate. Since our conclusions are based on the analysis of the upper part of the difference profile, we may regard it as reliably established that the angular distribution of the noise takes the form of a "lens" which is oblate in the direction of the magnetic field and has equal amplitudes in the  $r$  and  $\varphi$  directions.

4. The spatial noise distribution which we have established corresponds to the development of turbulence with circularly polarized electric field vector and frequencies  $\omega \ll 10^{11}$  sec $^{-1}$ . The current flowing across the

magnetic field excites in this frequency region an instability with similar angular distributions at the lower hybrid frequency<sup>[12,13]</sup> and at the harmonics of the electron cyclotron frequency.<sup>[14]</sup> As regards the low-frequency instabilities,<sup>[12,13]</sup> our previous measurements<sup>[10]</sup> enable us to conclude that the corresponding electric fields do not exceed  $\tilde{E} \approx 100$  V/cm, i.e., they are very much smaller than those measured spectroscopically in the present work. The instability development<sup>[14]</sup> is therefore most probable at frequencies<sup>2)</sup>  $\omega = n\omega_{He} - \mathbf{k} \cdot \mathbf{v}$ .

However, this hypothesis leads to certain difficulties when the measured noise level is compared with theoretical calculations<sup>[14,15]</sup> for homogeneous plasma: the measured noise level turns out to be much higher than one would expect theoretically. In all probability, the simultaneous development of low-frequency<sup>[12]</sup> and high-frequency<sup>[14,15]</sup> noise in the zero layer is accompanied by a nonlinear interaction between them which disturb the homogeneity of the plasma and leads to the enhancement oscillations with  $\omega = n\omega_{He} - \mathbf{k} \cdot \mathbf{v}$ .

The measured amplitudes of longitudinal noise oscillations were found to be substantially lower than the transverse noise amplitudes but still greater than the mean interparticle fields  $E_0 = 2.6eN^{2/3}$ . This means that, in addition to the noise considered above, the plasma may also support noise with fields  $\tilde{E} \leq 8$  kV/cm, whose angular distribution lies mainly along the current flow. In principle, this level of ion-acoustic noise is sufficient to explain the anomalous collision frequency in the zero layer.

It is our pleasant duty to express our grateful thanks to Academician E. K. Zavoiskii for his constant interest and attention, and to L. I. Rudakov for many useful discussions.

<sup>1)</sup>For the sake of simplicity we shall write  $\langle E_{||}^2 \rangle \equiv E_z^2$ ,  $1/2 \langle E_{\perp}^2 \rangle \equiv E_x^2$ .

<sup>2)</sup>We note, by the way, that in the coordinate system in which the ions and neutral atoms are at rest, the frequency of these unstable oscillations may turn out to be relatively low ( $\omega \lesssim 10^9$  sec) because of the Doppler effect, so that the true quasistatic condition is satisfied for the profile as a whole.

<sup>1)</sup>M. M. Butslav, A. G. Plakhov, V. V. Shapkin, and N. M. Yashin, *Opt. Spektrosk.* **16**, 2 (1964).

<sup>2)</sup>E. K. Zavoiskii and G. E. Smolkin, *Sb. Soveshchanie po diagnostike vysokotemperaturnoi plazmy, Sukhumi* (in: *Conf. on High-Temperature Plasma Diagnostics, Sukhumi*) Atomizdat, 1970, p. 40.

<sup>3)</sup>G. V. Sholin, *Dokl. Akad. Nauk SSSR* **195**, 589 (1970) [*Sov. Phys.-Doklady* **15**, 1040 (1971)].

<sup>4)</sup>S. P. Zagorodnikov, G. E. Smolkin, E. A. Striganova, and G. V. Sholin, *ZhETF Pis. Red.* **11**, 475 (1970) [*JETP Lett.* **11**, 323 (1970)]; *Dokl. Akad. Nauk SSSR* **195**, 1065 (1970) [*Sov. Phys.-Doklady* **15**, 1122 (1971)].

<sup>5)</sup>E. K. Zavoiskii, Yu. G. Kalinin, V. A. Skoryupin, V. V. Shapkin, and G. V. Sholin, *Dokl. Akad. Nauk SSSR* **194**, 55 (1970) [*Sov. Phys.-Doklady* **15**, 823 (1971)].

<sup>6)</sup>L. P. Zakatov, A. G. Plakhov, G. V. Shapkin, and G. V. Sholin, *Dokl. Akad. Nauk SSSR* **198**, 1306 (1971) [*Sov. Phys.-Doklady* **16**, 451 (1971)].

<sup>7)</sup>E. K. Zavoiskii, Yu. G. Kalinin, V. A. Skoryupin, V. V. Shapkin and G. V. Sholin, *ZhETF Pis. Red.* **13**, 19 (1971) [*JETP Lett.* **13**, 12 (1971)].

<sup>8)</sup>I. I. Sobel'man, *Vvedenie v teoriyu atomnykh spektrov* (Introduction to the Theory of Atomic Spectra), Fizmatgiz, 1963.

<sup>9)</sup>G. V. Sholin and E. A. Oks, *Dokl. Akad. Nauk SSSR* **209**,

- No. 6 (1973) [Sov. Phys.-Doklady 18, No. 4 (1973)].
- <sup>10</sup>M. V. Babykin, A. I. Zhuzhunashvili, and S. S. Sobolev, Zh. Eksp. Teor. Fiz. 60, 345 (1971) [Sov. Phys.-JETP 33, 188 (1971)].
- <sup>11</sup>L. I. Rudakov and L. V. Korablev, Zh. Eksp. Teor. Fiz. 50, 220 (1966) [Sov. Phys.-JETP 23, 145 (1966)].
- <sup>12</sup>V. I. Aref'ev, A. V. Gordeev, and L. I. Rudakov, Plasma Phys. and Controlled Nucl. Fus. Research, Vol. II, IAEA, Vienna, 1969, p. 165.
- <sup>13</sup>N. A. Kroll and P. C. Liewer, Phys. Rev. 4A, 2094 (1971).
- <sup>14</sup>P. Forslund, R. Morse, and C. Nielson, Phys. Fluids 15, 1303 (1972).
- <sup>15</sup>A. A. Galeev, D. G. Lominadze, A. D. Pataraya, R. Z. Sagdeev, and K. N. Stepanov, ZhETF Pis. Red. 15, 417 (1972) [JETP Lett. 15, 294 (1972)].

Translated by S. Chomet  
19